



## The discovery of potent and selective pyridopyrimidin-7-one based inhibitors of B-Raf<sup>V600E</sup> kinase

Li Ren<sup>a,\*</sup>, Kateri A. Ahrendt<sup>a</sup>, Jonas Grina<sup>a</sup>, Ellen R. Laird<sup>a</sup>, Alex J. Buckmelter<sup>a</sup>, Joshua D. Hansen<sup>a</sup>, Brad Newhouse<sup>a</sup>, David Moreno<sup>a</sup>, Steve Wenglowsky<sup>a</sup>, Victoria Dinkel<sup>a</sup>, Susan L. Gloor<sup>a</sup>, Gregg Hastings<sup>a</sup>, Sumeet Rana<sup>a</sup>, Kevin Rasor<sup>a</sup>, Tyler Risom<sup>a</sup>, Hillary L. Sturgis<sup>a</sup>, Walter C. Voegtli<sup>a</sup>, Simon Mathieu<sup>b</sup>

<sup>a</sup>Array BioPharma, Inc., 3200 Walnut Street, Boulder, CO 80301, United States

<sup>b</sup>Genentech, Inc., 1 DNA Way, South San Francisco, CA 94080-4990, United States

### ARTICLE INFO

#### Article history:

Received 22 February 2012

Revised 29 March 2012

Accepted 3 April 2012

Available online 10 April 2012

#### Keywords:

B-Raf

Kinase

Drug discovery

Pyridopyrimidin-7-one

Structure based drug design

### ABSTRACT

Herein we describe the discovery of a novel series of ATP competitive B-Raf inhibitors via structure based drug design (SBDD). These pyridopyrimidin-7-one based inhibitors exhibit both excellent cellular potency and striking B-Raf selectivity. Optimization led to the identification of compound **17**, a potent, selective and orally available agent with excellent pharmacokinetic properties and robust tumor growth inhibition in xenograft studies.

© 2012 Elsevier Ltd. All rights reserved.

The Raf family protein kinases, consisting of A-Raf, B-Raf, and C-Raf, are central components of the MAPK pathway that regulates cellular proliferation, differentiation, and survival.<sup>1</sup> Raf kinases act downstream of RAS and are responsible for MEK and ERK activation. BRAF gene mutations may lead to MAPK pathway amplification via constitutive activation of B-Raf, and are present in ~7% of all cancers,<sup>2</sup> with high frequency in malignant melanoma (30–70%).<sup>3,4</sup> The most common (>90%) mutation in B-Raf is a glutamic acid for valine substitution at residue 600 (V600E),<sup>2</sup> which leads to constitutive kinase activity 500-fold greater than wild-type B-Raf,<sup>5</sup> and correlates with increased malignancy and decreased response to chemotherapy.<sup>6</sup> A number of drug candidates targeting the B-Raf<sup>V600E</sup> mutation have entered clinical trials in recent years. Several of these, such as vemurafenib<sup>7</sup> and dabrafenib<sup>8</sup> have shown clinical efficacy, thus validating B-Raf<sup>V600E</sup> as a cancer target.

Our lab recently reported the discovery of several novel series of potent and selective inhibitors of B-Raf<sup>V600E</sup>.<sup>9</sup> A common feature for these inhibitors (Fig. 1) is an amide linker connecting various hinge-binding templates to an aryl sulfonamide, with the amide –NH making a weak hydrogen bond to the hydroxyl of the gate-

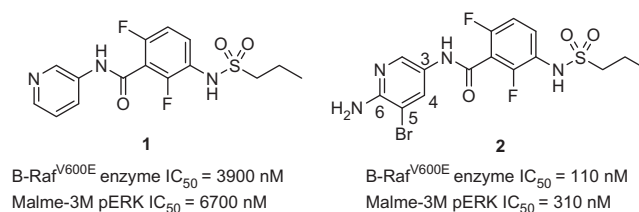


Figure 1. B-Raf<sup>V600E</sup> inhibitors **1** and **2**.

keeper residue Thr529.<sup>9a</sup> The initial series of amide-linked B-Raf<sup>V600E</sup> inhibitors utilized a pyridine as a hydrogen bond acceptor, which was postulated to bind to the –NH of hinge residue Cys532. The micromolar enzymatic and cellular activity of pyridine amide **1** was improved 30-fold by introducing an amino group at the 6-position and a bromine atom at the 5-position.<sup>9a</sup>

An X-ray crystal structure<sup>9a</sup> of B-Raf<sup>WT</sup> in complex with amino pyridine amide **2** revealed that the newly installed 6-amino group is hydrogen-bonded to the carbonyl of Cys532, the sulfonamide moiety forms several hydrogen bonds with the backbone of the DFG sequence, and the propyl chain occupies a small lipophilic pocket that is enlarged by an outward shift of the  $\alpha\text{C}$ -helix (Fig. 2).

The bromine atom makes key lipophilic contacts to the side chains of Ile463, Val471, Trp531, and Phe583.

\* Corresponding author.

E-mail address: [li.ren@arraybiopharma.com](mailto:li.ren@arraybiopharma.com) (L. Ren).

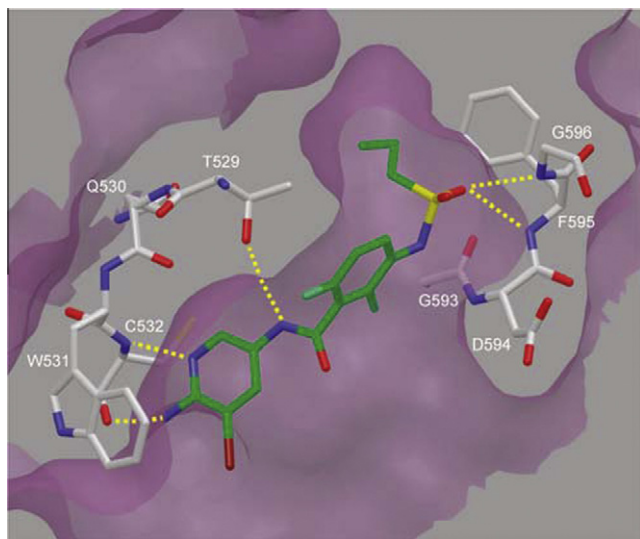


**Figure 2.** X-ray crystal structure of **2** in complex with B-Raf<sup>WT</sup>. The cleft surface is rendered in violet, select residues are depicted in white, and the inhibitor is green. Hydrogen-bonding interactions are illustrated with yellow dashed lines. Several residues that are involved in hydrophobic interactions with **2** are omitted for clarity and are described in the text. The propyl group resides in a pocket that is enlarged by an outward shift of the  $\alpha$ C-helix. The DFG sequence (D594–G596) resides in its active (DFG-in) conformation.

The crystal structure also revealed two characteristic conformational features of the amide series: a near co-planar arrangement of the amide group with the hinge-binding scaffold and a near 90° torsion angle of the amide relative to the 2,6-di-halo substituted central phenyl ring. This resulted in a near orthogonal spatial arrangement between the propylsulfonamide bearing phenyl ring and the hinge-binding pyridine ring, and positions them to interact optimally with residues in the ATP pocket. Although the amide linker functioned efficiently as a spacer and a conformational control, its chemical and metabolic stability were perceived as liabilities. Indeed, potentially toxic aniline metabolites generated from in vivo cleavage of the amide bond were observed. To address these concerns, we initiated a program to identify alternative linkers.

Our strategy was based on the observation that the amide linker adopted a near co-planar conformation in relationship to the pyridine ring. Wishing to retain the propyl sulfonamide moiety, a key feature for the DFG-in/ $\alpha$ C-helix shifted binding mode, we explored the approach of connecting the amide to the 4-position of the pyridine to form a fused heterocycle (Fig. 3). The resulting inhibitor with the appropriate torsion angle between the newly introduced bicycle and the propylsulfonamide bearing phenyl ring should maintain all the critical interactions with the enzyme.

Due to synthetic accessibility, initial hinge-binding template evaluation focused on fused heterocycles with a single hinge contact to the main chain –NH of Cys532. It was anticipated that once an optimal scaffold was identified, activity could be further improved 4- to 5-fold by installing an amino group at the appropriate position to interact with the carbonyl of Cys532.<sup>9a</sup> Selected examples are shown in Table 1.<sup>10</sup>

Pyrrolopyridine **3** was prepared in an attempt to retain the amide –NH interaction with the gatekeeper residue Thr529, but

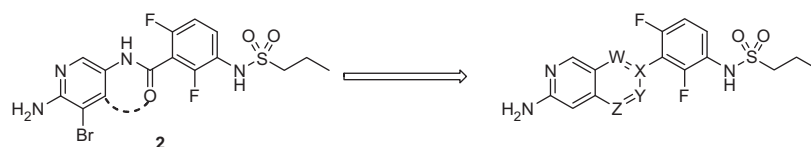


**Figure 3.** Schematic illustration of the amide linker replacement strategy.

**Table 1**  
B-Raf activity of compounds **3–9**

Compd	Ar	B-Raf <sup>V600E</sup> IC <sub>50</sub> <sup>a</sup> (nM)	pERK IC <sub>50</sub> <sup>a</sup> (nM)
<b>3</b>		>10,000	— <sup>b</sup>
<b>4</b>		340	— <sup>b</sup>
<b>5</b>		3606	— <sup>b</sup>
<b>6</b>		241	703
<b>7</b>		72	469
<b>8</b>		71	445
<b>9</b>		13	1163

<sup>a</sup> IC<sub>50</sub> values reflect the average from at least two separate experiments.

<sup>b</sup> Not determined.

was inactive. Modeling studies revealed that the 6,5-fused ring system repositioned the central di-halo aryl ring and the propylsulfonamide tail, rendering **3** unable to maintain key contacts with the DFG motif. In contrast, molecular modeling suggested that the propyl sulfonamide on the 6,6-fused template should occupy a similar space when compared to the amide series. As predicted, isoquinoline **4**, showed ca. 10-fold improvement in enzyme inhibition over **1**. The new core also made an improved hydrophobic contact with Phe583 on the floor of the ATP pocket. Incorporating a nitrogen atom into the second ring made a striking difference to activity depending on the substitution pattern. Compound **5** was less active most likely owing to a desolvation penalty upon burial of a strong hydrogen bond acceptor. Binding activity was restored for 2,6-naphthyridine **6**, where N2 is more accessible to solvent, with concomitant submicromolar cellular activity. Consistent with the observation made in the amide series, 8-bromo naphthyridine **7** showed improved potency presumably due to added hydrophobic contacts with the protein. Further improvement over **6** could also be achieved by introducing a carbonyl group into the second ring. The resulting 2,6-naphthyridin-1-one **8** showed similar activity to **7**. Finally, 1,6-naphthyridin-2-one **9**, an inhibitor with reversed amide connectivity, showed the most promising enzyme activity. Results from modeling of compound **9** suggested that the potency gain could be attributed to improved hydrophobic contact between the phenethyl substituent on the amide nitrogen and residues of the P-loop (Fig. 4).

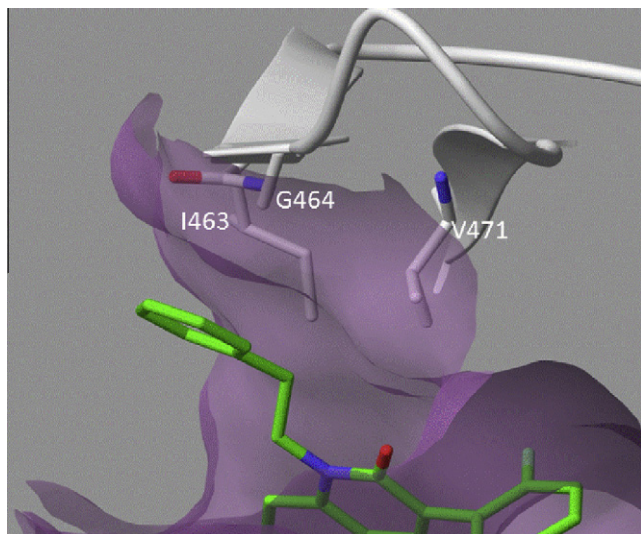


**Figure 4.** Model of **9** illustrating the possibility for hydrophobic contact between residues of the P-loop and the phenethyl group.

Subsequent optimization focused on 6,6-fused bicyclic systems represented by compounds **4**, **6**, **8**, and **9** due to their initial encouraging activities. As pointed out earlier, targeting the interaction with the carbonyl of Cys532 via an amino group became the next priority. However, the considerable synthetic challenges associated with **6** and **8** precluded further investigation of these scaffolds. Selected examples from expansion of templates **4** and **9** are shown in Table 2.

Amino isoquinoline **10**, with an appropriately placed NH<sub>2</sub> moiety, showed no improvement in enzyme potency over **4**. Increased activity was observed for **11**, by converting the hinge-binding motif in **10** from an isoquinoline to a quinazoline. The potency of the aminoquinazoline scaffold could be further enhanced via the strategy that was employed previously (**9** vs **4**). The resulting pyridopyrimidin-7-one analog **12** showed encouraging activity in both enzyme and cellular assays, and served as a starting point for further optimization.

In parallel to the on-going efforts to identify an optimal bi-aryl template to replace the amide linker, the effect of varying the substitutions at the 2 and 6-position on the central phenyl ring was briefly evaluated with the aminoquinazoline series (Table 3).

Removing both fluorines (**13**) completely abolished any B-Raf activity and a mono-fluoro at the 6-position (**14**) was also inactive.

**Table 2**  
B-Raf activity of compounds **10–12**

Compd	Ar	B-Raf <sup>V600E</sup> IC <sub>50</sub> <sup>a</sup> (nM)	pERK IC <sub>50</sub> <sup>a</sup> (nM)
<b>10</b>		549	— <sup>b</sup>
<b>11</b>		140	682
<b>13</b>		10	93

<sup>a</sup> IC<sub>50</sub> values reflect the average from at least two separate experiments.

<sup>b</sup> Not determined.

**Table 3**  
B-Raf activity of compounds **11**, **13–15**

Compd	R <sub>1</sub> , R <sub>2</sub>	B-Raf <sup>V600E</sup> IC <sub>50</sub> <sup>a</sup> (nM)	pERK IC <sub>50</sub> <sup>a</sup> (nM)
<b>11</b>	F, F	140	682
<b>13</b>	H, H	>10,000	— <sup>b</sup>
<b>14</b>	H, F	>10,000	— <sup>b</sup>
<b>15</b>	H, Me	128	>10,000

<sup>a</sup> IC<sub>50</sub> values reflect the average from at least two separate experiments.

<sup>b</sup> Not determined.

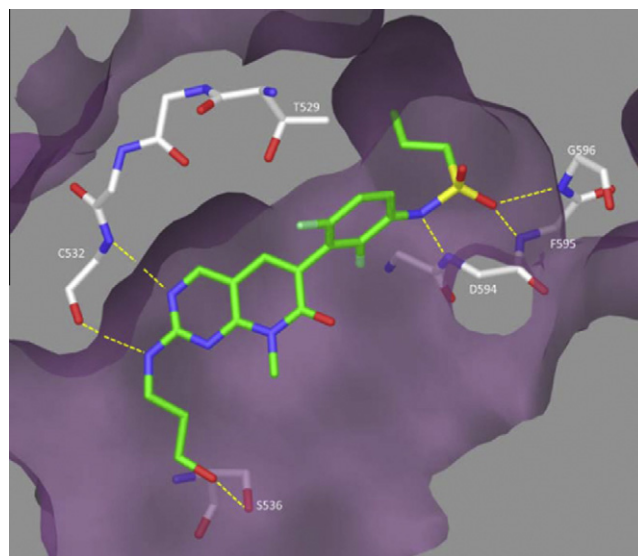


**Figure 5.** X-ray crystal structure of **19** in complex with B-Raf<sup>WT</sup>. The color scheme is as described in Figure 2, and the observed interactions are consistent with those depicted for compound **2**. The hydroxypropyl group is involved in a hydrogen bond with the sidechain of Ser536.

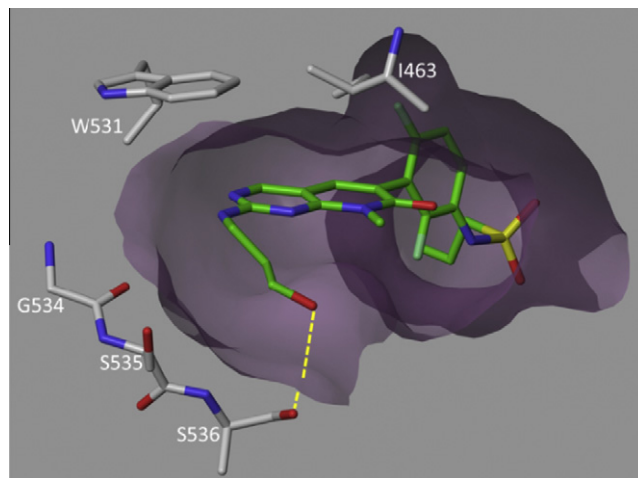
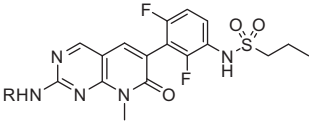


**Figure 6.** Edge view of the X-ray crystal structure of **19** illustrating the added contacts at the exit of the ATP cleft. Several of these residues are expected to be involved in the potency enhancements for compounds described in Table 4.

**Table 4**  
B-Raf activity of compounds **12**, **16**–**23**



Compd	R	B-Raf <sup>V600E</sup> IC <sub>50</sub> <sup>a</sup> (nM)	pERK IC <sub>50</sub> <sup>a</sup> (nM)
<b>12</b>	H	10	93
<b>16</b>	Me	9	45
<b>17</b>		3	27
<b>18</b>	CH <sub>2</sub> CH <sub>2</sub> OH	6	31
<b>19</b>	CH <sub>2</sub> CH <sub>2</sub> CH <sub>2</sub> OH	7	41
<b>20</b>		15	73
<b>21</b>	Ph	0.5	5
<b>22</b>	3-Pyridyl	0.5	3
<b>23</b>	1-Methyl-pyrazole-4-yl	0.4	1

<sup>a</sup> IC<sub>50</sub> values reflect the average from at least two separate experiments.

These results indicate that the 2-substituent is critical for potency and are consistent with SAR from the amide series.<sup>9b</sup> Although the enzyme potency of **15** is equivalent to **11**, the 6-methyl derivative lacks any cellular activity. While the exact reason favoring the 2,6-difluoro substitution pattern is unclear, possible explanations include effects of the fluorines on hydrophobic contacts, torsion angle, and/or the pK<sub>a</sub> of the sulfonamide motif.

The similar SAR trends from two distinct series on the central phenyl ring convinced us to use the 2,6-difluoro phenyl sulfonamide tail for the optimization of the pyridopyrimidin-7-one scaffold.

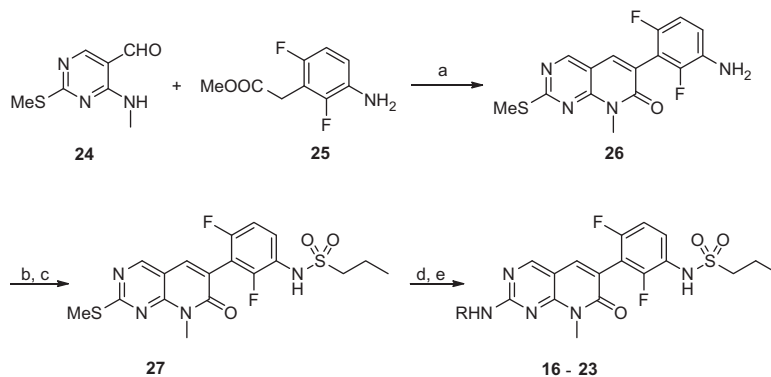
fold. We reasoned that further improvement in potency could be achieved by exploring contacts to the outer edge of the ATP cleft (defined by residues Gly534-Ser536, and the sidechains of Ile463, Trp531); illustrated in Figure 6 (vide infra); selected examples are shown in Table 4.

Alkyl substitutions in general gave a 2- to 3-fold improvement in cell potency over **12**. The most potent among these was compound **17**, a cyclopropylmethyl derivative with a pERK IC<sub>50</sub> of 27 nM. Installation of aryl and heteroaryl groups resulted in the identification of several highly active B-Raf inhibitors, several of which exhibited sub-nanomolar enzyme activity with single digit nanomolar cellular potency. For instance, compound **23** showed an impressive pERK IC<sub>50</sub> of 1 nM.

An X-ray crystal structure of B-Raf<sup>WT</sup> in complex with **19** confirmed our anticipated binding mode and the hydroxypropyl group is involved in a hydrogen bond with the sidechain of Ser536 (Fig. 5).<sup>11</sup>

The pyridopyrimidin-7-ones were prepared according to Scheme 1. Condensation of 4-(methylamino)-2-(methylthio)pyrimidine-5-carbaldehyde **24** with methyl 2-(3-amino-2,6-difluorophenyl)acetate **25** in the presence of K<sub>2</sub>CO<sub>3</sub> afforded 6-(3-amino-2,6-difluorophenyl)-8-methyl-2-(methylthio)pyrido[2,3-*d*]pyrimidin-7(8*H*)-one **26**. Mono-sulfonation of aniline **26** was accomplished in a two-step fashion to give **27**. Activation of the methylthio moiety via oxidation, followed by displacement with amines furnished compounds **16**–**23**.

Due to their potent cellular activity, **21**–**23** were screened in a panel of 65 protein kinases at 1 μM. Unfortunately, these analogs showed strong inhibition (>90%) of multiple kinases such as ABL, FGR, KDR, LCK and SRC. These findings were consistent with literature reports on PD166285,<sup>12</sup> a related compound without the propylsulfonamide, which is a multi-kinase inhibitor. On the contrary, alkyl derivatives **17**, **18** and **19** exhibited excellent kinase selectivity toward non-Raf kinases. For example, the inhibitory activity of



**Scheme 1.** Preparation of pyridopyrimidin-7-ones: Reagents and conditions: (a) K<sub>2</sub>CO<sub>3</sub>, DMF, 80 °C; (b) *n*-PrSO<sub>2</sub>Cl, NEt<sub>3</sub>, DCM; (c) NaOH, MeOH/THF; (d) *m*-CPBA, DCM; (e) NH<sub>2</sub>R, 90 °C.

**Table 5**  
In vitro ADME and pharmacokinetic properties of **17**–**19**

Compd	Caco-2 <sup>b</sup>	Hepatocyte clearance <sup>a</sup>	Observed clearance <sup>c</sup>	V <sub>d</sub> <sup>d</sup>	AUC <sup>f</sup>	%F
<b>17</b>	High	17	3	0.46	133	33
<b>18</b>	High	75	74	1	1	18
<b>19</b>	High	46	— <sup>e</sup>	20	20	— <sup>e</sup>

<sup>a</sup> Mouse hepatocyte clearance (ml/min/kg).

<sup>b</sup> Caco-2 permeability classification: low (<2 × 10<sup>-6</sup> cm/s), medium (2–8 × 10<sup>-6</sup> cm/s), high (>8 × 10<sup>-6</sup> cm/s).

<sup>c</sup> Mouse IV PK at 2.5 mg/kg (ml/min/kg).

<sup>d</sup> l/kg.

<sup>e</sup> Not determined.

<sup>f</sup> Mouse PO PK at 30 mg/kg (μM h).

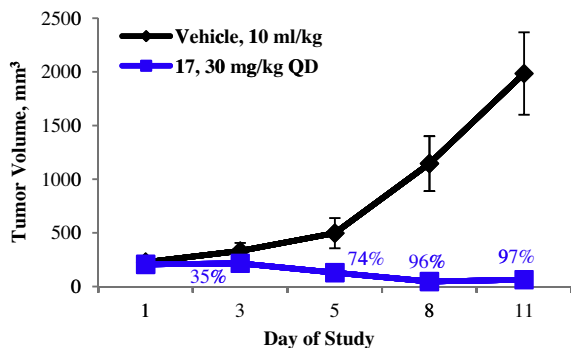


Figure 7. Tumor growth inhibition of 17 in LOX xenograft.

17 was assessed at 1  $\mu\text{M}$  against a panel of 228 kinases from across the human kinome at  $[\text{ATP}] \sim K_{m, \text{ATP}}$ . Only one kinase (LIMK1) showed >80% inhibition at 1  $\mu\text{M}$  besides B-Raf and C-Raf.

Compounds 17–19 were highly permeable in a Caco-2 permeability assay and showed variable stability in mouse hepatocytes (Table 5). Importantly, the most stable analog 17 exhibited low clearance in mouse pharmacokinetic studies and afforded the highest oral exposure level. On the contrary, the least stable derivative 18 showed high clearance with very low AUC.

Based on the optimal combination of activity and pharmacokinetic properties, 17 was advanced to a tumor growth inhibition (TGI) study in nude mice with established LOX (B-Raf<sup>V600E</sup>) xenografts. Compound 17 was administered at a daily dose of 30 mg/kg QD from day 1 to day 4, and tumor volume was measured on day 1, 3, 5, 8, and 11 (Fig. 7). After 4 days of dosing, a 74% TGI response was registered on day 5. More importantly, prolonged inhibition was observed even after dosing was stopped. For example, 96% & 97% TGI were reported on day 8 and 11. These findings suggest that compound 17 is a highly efficacious B-Raf inhibitor.

In summary, using structure based drug design (SBDD), we have discovered a series of pyridopyrimidin-7-one-based B-Raf inhibitors with excellent potency and selectivity profiles. Optimization led to the identification of compound 17, a potent, selective and orally available B-Raf inhibitor with excellent pharmacokinetic properties and robust tumor growth inhibition in xenograft studies.

## Acknowledgments

The authors thank Susan Rhodes and Jennifer Otten for Caco-2 determinations. The authors also thank Dr. Joachim Rudolph for critical review of the manuscript and helpful suggestions.

## References and notes

1. Peyssonnaud, C.; Eychene, A. *Biol. Cell.* **2001**, *93*, 53.
2. Davies, H.; Bignell, G. R.; Cox, C.; Stephens, P.; Edkins, S.; Clegg, S.; Teague, J.; Woffendin, H.; Garnett, M. J.; Bottomley, W.; Davis, N.; Dicks, E.; Ewing, R.; Floyd, Y.; Gray, K.; Hall, S.; Hawes, R.; Hughes, J.; Kosmidou, V.; Menzies, A.; Mould, C.; Parker, A.; Stevens, C.; Watt, S.; Hooper, S.; Wilson, R.; Jayatilake, H.; Gusterson, B. A.; Cooper, C.; Shipley, J.; Hargrave, D.; Pritchard-Jones, K.; Maitland, N.; Chenevix-Trench, G.; Riggins, G. J.; Bigner, D. D.; Palmieri, G.; Cossu, A.; Flanagan, A.; Nicholson, A.; Ho, J. W. C.; Leung, S. Y.; Yuen, S. T.; Weber, B. L.; Seigler, H. F.; Darrow, T. L.; Paterson, H.; Marais, R.; Marshall, C. J.; Wooster, R.; Stratton, M. R.; Futreal, P. A. *Nature* **2002**, *417*, 949.
3. Pollock, P. M.; Harper, U. L.; Hansen, K. S.; Yudd, L. M.; Stark, M.; Robbins, C. M.; Moses, T. Y.; Hostetter, G.; Wagner, U.; Kakareka, J.; Salem, G.; Pohida, T.; Heenean, P.; Duray, P.; Kallioniemi, O.; Hayward, N. K.; Trent, J. M.; Meltzer, P. S. *Nat. Genet.* **2003**, *33*, 19.
4. (a) Gorden, A.; Osman, I.; Gai, W.; He, D.; Huang, W.; Davidson, A.; Houghton, A. N.; Busam, K.; Polsky, D. *Cancer Res.* **2003**, *63*, 3955; (b) Kuman, R.; Angelini, S.; Czene, K.; Sauroja, I.; Hahka-Kemppinen, M.; Pyrhonen, S.; Hemminki, K. *Clin. Cancer Res.* **2003**, *9*, 3362.
5. Wan, P. T.; Garnett, M. J.; Roe, S. M.; Lee, S.; Niculescu-Duvaz, D.; Good, V. M.; Jones, C. M.; Marshall, C. J.; Springer, C. J.; Barford, D.; Marais, R. *Cell* **2004**, *116*, 855.
6. (a) Samowitz, W. S.; Sweeney, C.; Herrick, J.; Albertsen, H.; Levin, T. R.; Murtaugh, M. A.; Wolff, R. K.; Slattey, M. L. *Cancer Res.* **2005**, *65*, 6063; (b) Riesco-Eizaguirre, G.; Gutiérrez-Martínez, P.; García-Cabezas, M. A.; Nistal, M.; Santisteban, P. *Endocr-Relat. Cancer* **2006**, *13*, 257; (c) Houben, R.; Becker, J. C.; Kappel, A.; Terheyden, P.; Bröcker, E. B.; Goetz, R.; Rapp, U. R. *J. Carcinog.* **2004**, *3*, 6.
7. Puzanov, I.; Flaherty, K. T.; Sosman, J. A.; Grippo, J. F.; Su, F.; Nolop, K.; Lee, R. J.; Bollag, G. *Drugs Fut.* **2011**, *36*, 191.
8. Kefford, F. F.; Arkenau, H.; Brown, M. P.; Millward, J. R.; Infante, J. R.; Long, G. V.; Ouellet, D.; Curtis, M.; Lebowitz, P. F.; Falchook, G. S. *J. Clin. Oncol.* **2010**, *28*, 8503. 15s Abstr.
9. (a) Wenglowksy, S.; Ren, L.; Ahrendt, K. A.; Laird, E. R.; Aliagas, I.; Alick, B.; Buckmelter, A. J.; Choo, E. F.; Dinkel, V.; Feng, B.; Gloor, S. L.; Gould, S. E.; Gross, S.; Gunzner-Toste, J.; Hansen, J. D.; Hatzivassiliou, G.; Liu, B.; Malesky, K.; Mathieu, S.; Newhouse, B.; Raddatz, N. J.; Ran, Y.; Rana, S.; Randolph, N.; Risom, T.; Rudolph, J.; Savage, S.; Selby, L. T.; Shrag, M.; Song, K.; Sturgis, H. L.; Voegtli, W. C.; Wen, Z.; Willis, B. S.; Woessner, R. D.; Wu, W.-I.; Young, W. B.; Grina, J. *ACS Med. Chem. Lett.* **2011**, *2*, 342; (b) Wenglowksy, S.; Ahrendt, K. A.; Buckmelter, A. J.; Feng, B.; Gloor, S. L.; Gradi, S.; Grina, J.; Hansen, J. D.; Laird, E. R.; Lunghofer, P.; Mathieu, S.; Moreno, D.; Newhouse, B.; Ren, L.; Risom, T.; Rudolph, J.; Seo, J.; Sturgis, H. L.; Voegtli, W. C.; Wen, Z. *Bioorg. Med. Chem. Lett.* **2011**, *21*, 5533; (c) Ren, L.; Laird, E.; Buckmelter, A. J.; Dinkel, V.; Gloor, S. L.; Grina, J.; Newhouse, B.; Rasor, K.; Hastings, G.; Gradi, S. N.; Rudolph, J. *Bioorg. Med. Chem. Lett.* **2012**, *22*, 1165; (d) Wenglowksy, S.; Moreno, D.; Rudolph, J.; Ran, Y.; Ahrendt, K. A.; Arrigo, A.; Colsen, B.; Gloor, S. L.; Hasting, G. *Bioorg. Med. Chem. Lett.* **2012**, *22*, 912.
10. Inhibitor enzyme activity was determined utilizing full-length B-Raf<sup>V600E</sup>. Inhibition of basal ERK phosphorylation in Malme-3M cells was used as the mechanistic cellular assay. For assay description see: Laird, E.; Lyssikatos, J.; Welch, M.; Grina, J.; Hansen, J.; Newhouse, B.; Olivero, A.; Topolav, G. WO 2006/084015 A2, 2006.
11. Coordinates for the B-Raf crystal structure have been deposited in the PDB: accession code 4E4X.
12. Panek, R. L.; Lu, G. H.; Klutchko, S. R.; Batley, B. L.; Dahring, T. K.; Hamby, J. M.; Hallak, H.; Doherty, A. M.; Keiser, J. A. *J. Pharmacol. Exp. Ther.* **1997**, *1433*.